PNAS RESEARCH ARTICLE | CHEMISTRY OPEN ACCESS

On the mechanisms of ion adsorption to aqueous interfaces: air-water vs. oil-water

Shane W. Devlin[a,b], Ilan Benjamin[c,1], and Richard J. Saykally[a,b,1]

Edited by Peter Rossky, Rice University, Houston, TX; received June 24, 2022; accepted September 1, 2022

The adsorption of ions to water-hydrophobe interfaces influences a wide range of phenomena, including chemical reaction rates, ion transport across biological membranes, and electrochemical and many catalytic processes; hence, developing a detailed understanding of the behavior of ions at water-hydrophobe interfaces is of central interest. Here, we characterize the adsorption of the chaotropic thiocyanate anion (SCN^-) to two prototypical liquid hydrophobic surfaces, water-toluene and water-decane, by surface-sensitive nonlinear spectroscopy and compare the results against our previous studies of SCN^- adsorption to the air-water interface. For these systems, we observe no spectral shift in the charge transfer to solvent spectrum of SCN^-, and the Gibb's free energies of adsorption for these three different interfaces all agree within error. We employed molecular dynamics simulations to develop a molecular-level understanding of the adsorption mechanism and found that the adsorption for SCN^- to both water-toluene and water-decane interfaces is driven by an increase in entropy, with very little enthalpic contribution. This is a qualitatively different mechanism than reported for SCN^- adsorption to the air-water and graphene-water interfaces, wherein a favorable enthalpy change was the main driving force, against an unfavorable entropy change.

ion adsorption | nonlinear spectroscopy | molecular dynamics | water-hydrophobe interactions

Significance

The Gibbs free energy of adsorption and interfacial electronic spectra of SCN^- (thiocyanate) ions at two water-liquid hydrophobe interfaces, water-toluene and water-decane, were measured with surface-sensitive spectroscopic techniques. Computer simulations revealed that the mechanism of ion adsorption to these interfaces is drastically different from those for other water-hydrophobe interfaces, viz. air-water and graphene-water.

Over the last two decades, our understanding of the nature of aqueous interfaces has evolved dramatically. It is now well accepted that certain ions preferentially adsorb to the interfacial region and can even have enhanced concentrations relative to the bulk (1, 2). That this ion behavior can have profound effects on the chemistry observed in the natural world is obvious. For example, the depletion of ozone at the surface of arctic sea ice (3, 4), the formation of acid rain and reactions in atmospheric aerosols (5, 6), and the uptake of CO_2 and other gases at the ocean surface (7) are all dynamic processes influenced by ion adsorption. Any attempt to understand these, and other, important systems must first establish a detailed understanding of the fundamental behavior of ions at interfaces.

To this end, nonlinear spectroscopies have been essential. Most commonly, the water structure adjacent to a hydrophobic phase is studied via vibrational sum-frequency generation (SFG), and chemical information is inferred by monitoring changes in the OH spectrum (8–13), as has been demonstrated by the Richmond, Allen, Roke, and Shen groups, among others. An alternative approach is to directly probe a suitable resonant ionic chromophore that resides in the interfacial layer, which can yield fundamental thermodynamic information regarding ion adsorption and solvation structure (14–20).

In addition, theoretical modeling of these systems has proven to be crucial for interpreting the spectroscopic data and developing a detailed chemical understanding of these interfaces. Along with the work of Jungwirth and Tobias, early theoretical studies focused on polarizability as the main driving force of ion adsorption (21, 22). Subsequently, more nuanced descriptions of ion adsorption included factors such as size, charge, volume exclusion, hydration enthalpy, and more (1, 21, 23–26). The challenge of uncoupling these parameters makes elucidating the forces driving ions to the interface a complex task. Accordingly, details regarding the mechanism of ion adsorption are still vigorously debated in the literature.

The Saykally and Geissler groups attempted to address these issues by combining temperature-dependent deep-ultraviolet (UV) second-harmonic generation (DUV-SHG) experiments and molecular dynamics (MD) simulations to determine the Gibb's free energy of adsorption for a prototypical, chaotropic anion to the air-water interface (23). They untangled the enthalpic and entropic components to the overall Gibb's free energy and proposed the following mechanism for anion adsorption: (1) *solvent repartitioning* provides the dominant negative enthalpic driving force. As the ion moves from the bulk to the interface, it sheds one or two of its weakly interacting solvating waters. These waters are then free to form stronger (more favorable) water-water hydrogen

Author affiliations: [a]Department of Chemistry, University of California, Berkeley, CA 94720; [b]Chemical Sciences Division, Lawrence Berkeley National Lab, Berkeley, CA 94720; and [c]Department of Chemistry, University of California, Santa Cruz, Santa Cruz, CA 95064

Author contributions: S.W.D., I.B., and R.J.S. designed research; S.W.D. I.B. performed research; S.W.D., I.B., and R.J.S. analyzed data; and S.W.D., I.B., and R.J.S. wrote the paper.

The authors declare no competing interest.

This article is a PNAS Direct Submission.

[1]To whom correspondence may be addressed. Email: ilan@ucsc.edu or saykally@berkeley.edu.

This article contains supporting information online at http://www.pnas.org/lookup/suppl/doi:10.1073/pnas.2210857119/-/DCSupplemental.

Published October 10, 2022.

bonds as part of the bulk-water network, compared with the weak ion-water interactions present in the solvation shell. (2) *Damping of capillary waves* (soft, collective fluctuations in surface topography) from the presence of the ion at the interface reduces entropy and impedes adsorption. This work highlighted the importance of hydration enthalpy as a main driving force for ion adsorption and helped to explain why strongly solvated ions, such as F^-, are largely repelled from the interfacial region, whereas weakly solvated ions, such as SCN^- and I^-, show enhanced interfacial concentrations.

An alternative mechanism of adsorption has been proposed by Wang et al., who studied the adsorption of a monovalent cation to the air-water interface (27). Qualitatively, they agreed that ion adsorption is an enthalpy-driven process; however, they attributed the negative enthalpy change to a decrease in pressure-volume ($P\Delta V$) work as the ion moves to the surface and not to solvent repartitioning. They also argued that the presence of the ion at the interface *increases* capillary wave fluctuations, rather than damping them (although they still report a net reduction in entropy, as the capillary wave fluctuations shift to occupy a single mode). Other studies of the air-water interface have examined the importance of hydration structure around the ion and electric field effects (28), as well as charge asymmetry of the liquid water surface (29).

Studies of *water-condensed hydrophobe* interfaces have also aided our understanding of the forces that drive ion adsorption. Saykally and Geissler extended their study of the air-water interface (23) by applying the same analysis to the graphene-water interface and determined a very similar Gibb's free energy, but revealing a qualitatively different mechanism of adsorption (14). Liquid-liquid interfaces have been studied with nonlinear and X-ray spectroscopies (9, 19, 30–35) as well as with MD simulation (36–40), and in certain cases, it has been shown that the structure/behavior of the air-water and water-liquid hydrophobe interfaces are quite similar (11, 36). Many of these studies have focused on ion transfer and solvent extraction, analyzing the effects that surfactants, anions, and cations have on fundamental properties such as the capillary width and ion pairing.

Based on these previous studies, we pose the question: what drives ion adsorption *to water-liquid hydrophobe interfaces*, and do these interfaces engender different mechanisms of adsorption, compared with air-water and graphene-water? In this work, we address this question by exploiting the inherently surface-specific techniques of broadband DUV electronic sum-frequency generation spectroscopy (DUV-ESFG) and resonantly enhanced DUV-SHG to characterize the adsorption of the thiocyanate anion (SCN^-) to two liquid hydrophobe interfaces, water-toluene and water-decane. We find that the interfacial charge transfer to solvent (CTTS) spectra for SCN^- at these interfaces are very nearly identical to that of air-water and that the Gibb's free energies of adsorption of all three interfaces are equal within error. MD simulations reveal that SCN^- adsorption to the decane-water and toluene-water interfaces is driven by an increase in the entropy of the system as the ion approaches the interface and that there is minimal enthalpic contribution. Thus, we reveal a strikingly different mechanism of adsorption than has been reported for the air-water and graphene-water interfaces and highlight the importance of accounting for molecular-level details when interpreting experimental data on ion adsorption.

Results and Discussion

Broadband DUV-ESFG Spectra. The bulk absorption spectrum of NaSCN in water is shown in Fig. 1*A* in the spectral window of 195–240 nm and comprises two CTTS transitions. Fox et al.

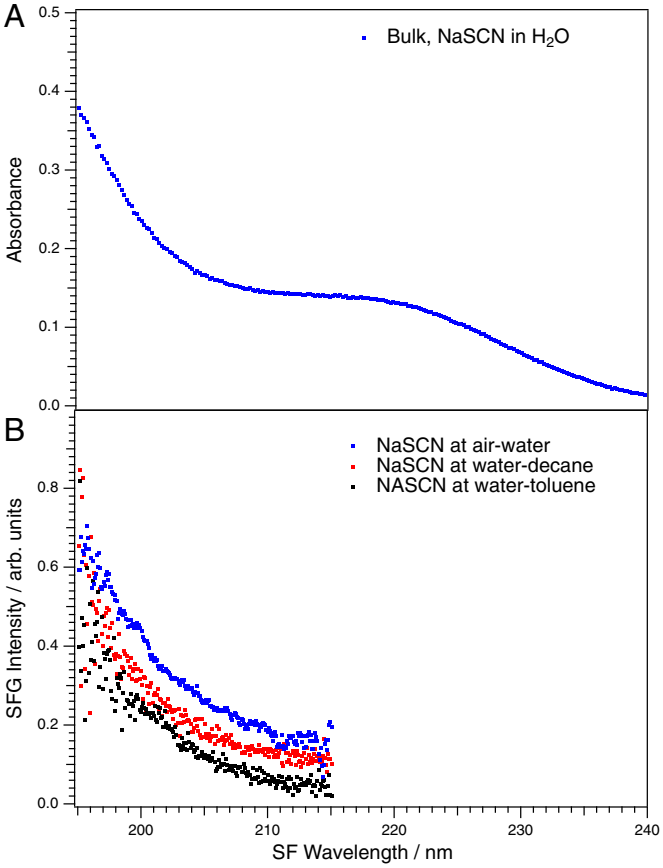

Fig. 1. Charge transfer to solvent (CTTS) spectra of (*A*) 100 μM NaSCN in bulk water and (*B*) 3M NaSCN at the air-water interface (blue dots), toluene-water interface (black dots), and decane-water interface (red dots). All three spectra in (*B*) overlap completely, but the air-water and decane-water spectra have been offset for viewing purposes. The interfacial CTTS spectra at the air-water and toluene-water interfaces have been published previously by Mizuno et al. (43) and Devlin et al. (15), respectively, and are reproduced here with permission from the authors.

measured the far-UV absorption spectrum of tetramethylammonium thiocyanate and assigned a lower energy transition centered at 216 nm and a higher-energy transition centered at 185 nm (41). The normalized, background-subtracted DUV-ESFG spectra of 3M NaSCN at the air-water (blue), decane-water (red), and toluene-water (black) interfaces are shown in Fig. 1*B*. As is evident by comparison between panels *A* and *B*, only the higher-energy transition is detectable with DUV-ESFG, the lower energy transition likely being two-photon inactive (an SFG selection rule), as has been observed for the CTTS transitions of other anions in water (42). The details of this have been discussed in a previous publication (43) and will not be a focus of the present study.

The key feature in Fig. 1*B* is the lack of any spectral shift of the higher-energy transition between these three unique interfaces. CTTS transitions are highly sensitive to local chemical environment, and any changes in solvation engendered by the differing interfaces would be expected to shift the higher-energy CTTS transition significantly. Even modest changes in solvent polarity have been shown to shift the bulk CTTS transitions of the iodide anion by 5 nm or more, a change easily measurable within the resolution of our detection system. We expect that the nonpolar hydrocarbons studied here would shift the transition significantly more than 5 nm. Indeed, Wang et al. have shown with SHG measurements that changes in surface polarity at liquid-liquid interfaces, such as water-chlorobenzene and

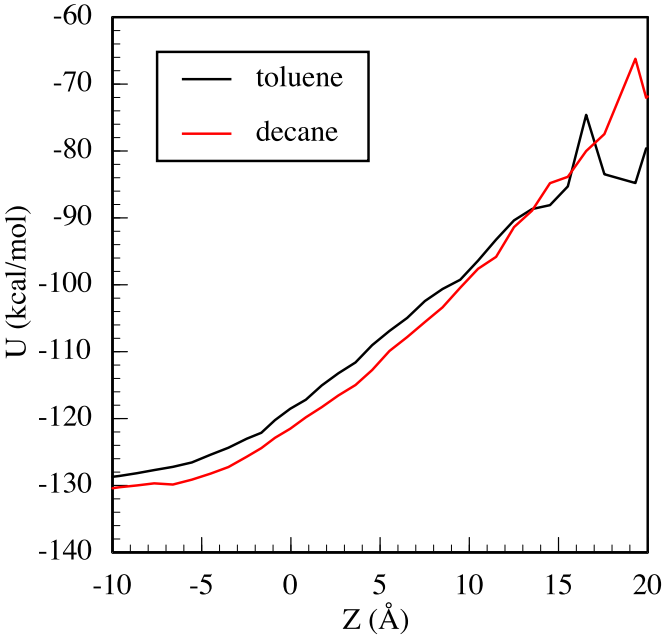

Fig. 2. The total interaction energy of the SCN^- ion with the water and the oil molecules for decane and toluene. Water-toluene data have been previously published and are reproduced here (66).

water-heptane, can shift charge transfer transitions of polarity indicator molecules by as much as 40 nm, compared with the air-water interface (17). The lack of a spectral shift observed here implies that the solvation environments around SCN^- at the air-water, toluene-water, and decane-water interfaces are strikingly similar and that the presence of the condensed oil phase induces very little perturbation. We support this finding through MD simulations by computing the interaction free energy of SCN^- with the water and oil molecules (Fig. 2) and show that it is remarkably similar for both the water-decane and water-toluene systems. More details on this are included in the next section.

Similar behavior for anions has been observed via other spectroscopic signatures. For example, it has been shown that the iodide and thiocyanate anions have insignificant changes in vertical ionization energies in bulk water vs. at the air-water interface, owing to the fact that these anions are asymmetrically solvated in bulk, which engenders similar solvation energetics as the geometrically constrained, asymmetric solvation environment at the interface (44).

SHG and the Langmuir Adsorption Model. The use of a Langmuir adsorption model to fit spectroscopic data are well established (2, 45, 46), and the methodology is adopted here for extracting the Gibb's free energy of adsorption from experimental SHG intensities. A thorough derivation of this model and its application to SHG is given in the *SI Appendix*. The measured second-harmonic (SH) intensities ($I_{2\omega}$) are related to the Gibb's free energy through the bulk anion concentration, according to the following:

$$I_{2\omega} = |\chi^{(2)}_{water} + \chi^{(2)}_{hydrocarbon} + \chi^{(2)}_{SCN^-}|^2 I^2_\omega \quad [1]$$

$$\frac{I_{2\omega}}{I^2_\omega} = |\chi^{(2)}|^2 \propto \left(A + B\frac{X_{SCN^-}}{(1-X_{SCN^-})e^{\frac{\Delta G}{RT}} + X_{SCN^-}} \right)^2 + \left(C\frac{X_{SCN^-}}{(1-X_{SCN^-})e^{\frac{\Delta G}{RT}} + X_{SCN^-}} \right)^2 \quad [2]$$

Here, $\chi^{(2)}_i$ is the second-order susceptibility of each species; I^2_ω is the fundamental intensity; A, B, and C are fitting parameters related to the nonresonant (real, A and B) and resonant (imaginary, C) components of the susceptibility for each species; X_{SCN^-} is the bulk concentration of SCN^-; and ΔG is the Gibb's free energy of adsorption.

It is important to consider the assumptions inherent to this Langmuir model and when they may break down in the systems studied here. First, the model assumes that only one adsorbate can bind to a surface "site," i.e., it describes monolayer coverage. At the higher concentrations used for these experiments, a monolayer is certainly surpassed, and contributions from the electric double layer should be considered. Second, the model assumes that all interfacial "sites" are treated equally, i.e., no interaction between adsorbing molecules are accounted for. Again, we expect this assumption to break down with increasing concentration; for example, the Debye length of a 0.1 M aqueous solution is ca. 1 nm; however, for a 2.5 M solution, it drops to 0.2 nm, and close-range interactions should be important. To that end, Venkateshwaran et al. have shown with simulation that water-mediated attraction between oppositely charged ions at the air-water interface is drastically enhanced compared with in bulk water (47). Despite these shortcomings, the Langmuir isotherm adequately models our experimental data and agrees with theoretical calculations, and we continue with its use instead of adopting a more complicated model.

Fig. 3 shows the normalized DUV-SHG intensities for SCN^- at the air-water, toluene-water, and decane-water interfaces plotted against bulk NaSCN concentration ranging from 0 to 2.5 M. The SCN^- CTTS transition has an extinction coefficient in the DUV of $\sim 10^4$ M^{-1} cm^{-1}, which provides strong resonance enhancement for these inherently weak second-order signals. The air-water and toluene-water data in Fig. 3*A* were collected at a SH wavelength of 193 nm, resulting in Gibbs free energies of adsorption of –7.5 ± 0.7 kJ/mol and –7.3 ± 0.7 kJ/mol, respectively. The air-water and decane-water data in Fig. 3*B* were collected at a SH wavelength of 200 nm, yielding Gibbs free energies of adsorption of –6.9 ± 0.8 kJ/mol and –6.7 ± 0.9 kJ/mol, respectively, with the uncertainties being one SD in the fit. All SHG intensities are normalized to the respective neat-water-hydrophobe interface, i.e., SHG = 1 for decane-water and toluene-water with no added salt.

The SHG intensity contains contributions from each component in the system: water, oil, and SCN^- (Eq. **1**). In the low concentration regime, the intensity increase with bulk anion concentration can be attributed to alignment of water molecules in the interfacial region, due to the static electric field from the ions (48). At higher concentrations, resonant enhancement from the anion begins to dominate as an electric double layer forms and appreciable SCN^- is present in the SHG probing depth. The exact probing depth is difficult to quantify experimentally; however, SHG is generated over the entire region with broken inversion symmetry, corresponding to roughly 1 nm for pure water and slightly deeper for electrolyte solutions (49).

The Gibb's free energy of adsorption for SCN^- to the air-water, toluene-water, and decane-water interfaces all agree within experimental error and are in good agreement with the free energy profiles calculated in Fig. 4. This behavior is consistent with previous measurements of anions at hydrophobic surfaces by the Saykally and Geissler groups, wherein the reported Gibb's free energies were all within error of that for air-water (14, 19, 20).

Free Energy Profile. The length scale of the ion's free energy change is determined, in part, by the density profiles of the water

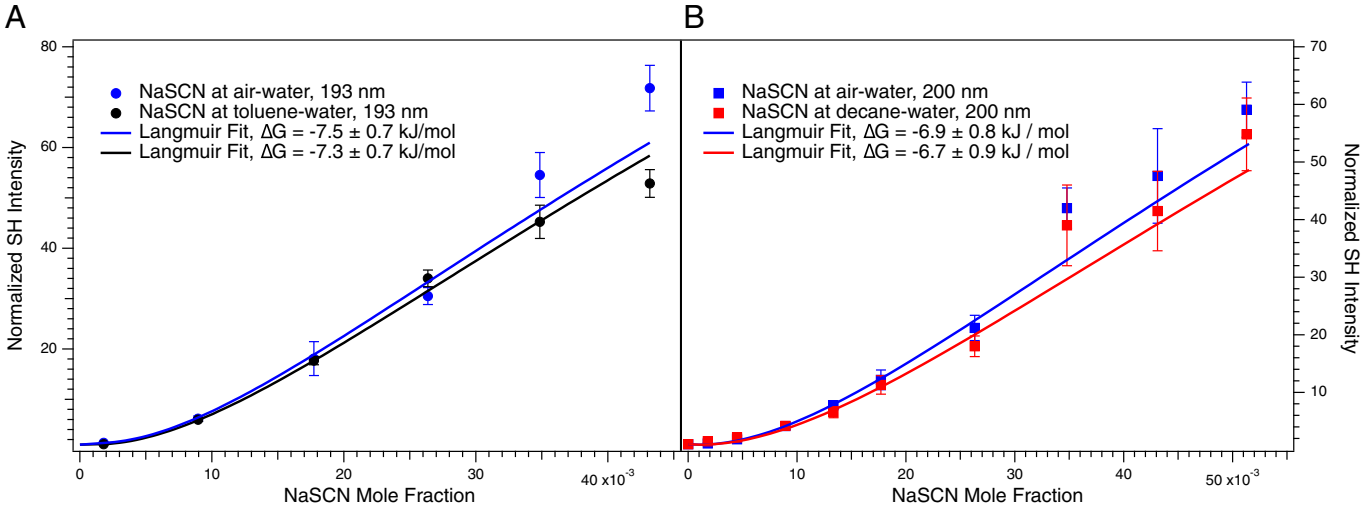

Fig. 3. Normalized second-harmonic generation (SHG) intensities versus bulk anion concentration. (*A*) Data for NaSCN at the air-water(blue circles) and toluene-water (black circles) interfaces collected at a SHG wavelength of 193 nm. (*B*) data for NaSCN at the air-water (blue squares) and decane-water (red squares) interfaces collected at a SHG wavelength of 200 nm. The lines represent the Langmuir adsorption fit to each respective data set, with the uncertainty being one SD. The data in (*A*) have been published previously by Devlin et al. and are reproduced here with permission from the authors (15).

and oil phases. The density profiles of neat water next to neat toluene and next to neat decane are shown in Fig. 5. $Z = 0$ is the location of the Gibbs dividing surface (GDS), which is the plane parallel to the interface where the water density is ∼50% of the bulk value. For an exact definition of the GDS, see for example Rowlinson and Widom (50). The so-called 90/10 interface region is defined as the distance over which the density of water declines from 90 to 10% of its bulk value and is quite narrow, about 4–5 Å.

The free energy profiles as the ion approaches the interface are shown in Fig. 4. The profile exhibits a small local minimum near the GDS that corresponds to a free energy of adsorption (relative to bulk water) of about –5.9 kJ/mol for both liquids, in reasonable agreement with the experimental values given above. As the ion crosses the interface, the free energy increases monotonically and rapidly (and will eventually reach a plateau significantly deep into the organic phase). The problem of ion transfer into the organic phases and the cotransfer of water molecules with the ion is outside the scope of this paper and will be described elsewhere. However, note that the more rapid rise in the free energy profile for decane, which signals a larger free energy of transfer of SCN^- across the water-decane interface than across the water-toluene interface, is consistent with the higher dielectric constant of toluene (2.4 compared with 2.0).

To gain insight into the nature of the identical local free energy minima observed for the two interfaces, we show in Fig. 2 the total interaction energy of the ion and the oil molecules. The lack of local minima in both cases suggests that the adsorption free energy is due to entropic contributions alone. This is markedly different from the results obtained for both the air-water and graphene-water interfaces. As the ion approaches the liquid-liquid interface, the existence of significant water structural fluctuations related to the ability of the ion to keep its hydration shell (51) results in an increase in disorder and thus significant entropic contribution to the free energy of adsorption. As the ion moves deeper into the organic phase, the significant loss in the energy of water hydration reduces the enthalpic contribution and causes the eventual increase in free energy. The increase in (negative) ion-oil interactions makes some enthalpic contributions, but not enough to offset the loss in the water hydration energy.

The free energy profiles shown in Fig. 4 and the change in energy of adsorption depicted in Fig. 2 suggest that the adsorption of the anion to the liquid-liquid interface is entropically driven. This can be understood as an increase in the water capillary fluctuations in the form of water "fingers" as the ion drags some of the hydration shell water molecules as it crosses the GDS. This phenomenon has been extensively documented for monoatomic ion transfer across the liquid-liquid interface (52–56) and is demonstrated in Fig. 6.

The formation of water "fingers" and the associated increase in entropy are rationalized in terms of the increase in water density fluctuations. The ion can be stabilized at the interface by a nearly complete hydration shell. The water molecules in the hydration shell are free to rapidly exchange with other nearby water molecules (57). Only when the ion is further

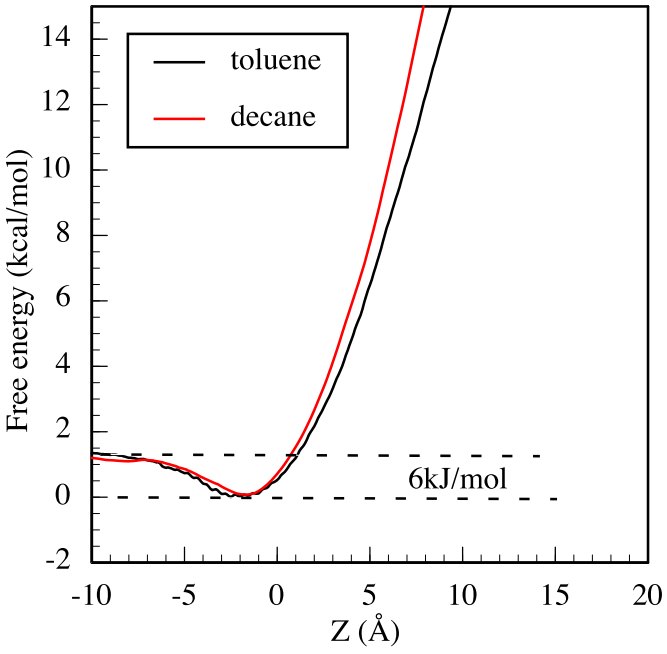

Fig. 4. The free energy profiles for moving the SCN^- ion across the water-toluene and water-decane interface at 298 K. Water-toluene data have been previously published and are reproduced here (66).

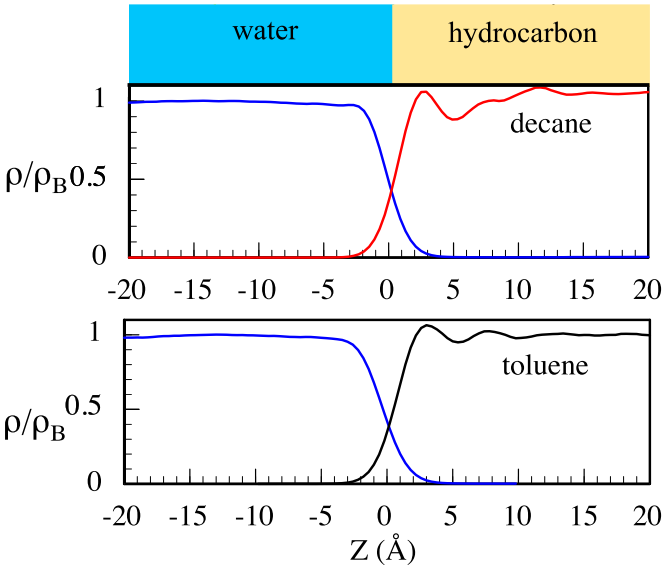

Fig. 5. Density profiles (relative to the respective bulk values) of water (blue) and oil at T = 298 K. $Z = 0$ is the location of the Gibbs dividing surface.

pushed into the oil phase does this process become less likely and the free energy rises rapidly.

Conclusions

The ubiquity of water-hydrophobe interactions in chemistry and biology necessitates a detailed understanding of these interfaces. In this work, we characterized the adsorption behavior of the SCN^- to two water-hydrophobe interfaces, water-toluene and water-decane, through resonantly enhanced nonlinear spectroscopy techniques. We report that the Gibb's free energy of adsorption and the interfacial CTTS spectra are in good agreement with these same measurements for SCN^- at the air-water and graphene-water interfaces. However, the details regarding the mechanism of adsorption are strikingly different. Specifically, we report that for the water-toluene and water-decane interfaces, ion adsorption is driven by an increase in entropy due to the formation of water "fingers" as the ion moves into the condensed organic phase, with very little enthalpic contribution.

Many studies have reported on the seemingly general behavior of water-hydrophobe interfaces (20, 36, 58–60). This work, along with others (14, 23), highlights the importance of accounting for specific, molecular-level details when studying ion adsorption to hydrophobic interfaces. This not only has profound impacts on our fundamental understanding of water-hydrophobe interactions, but also on how we apply this understanding to problems in chemistry, biology, atmospheric science, and other areas.

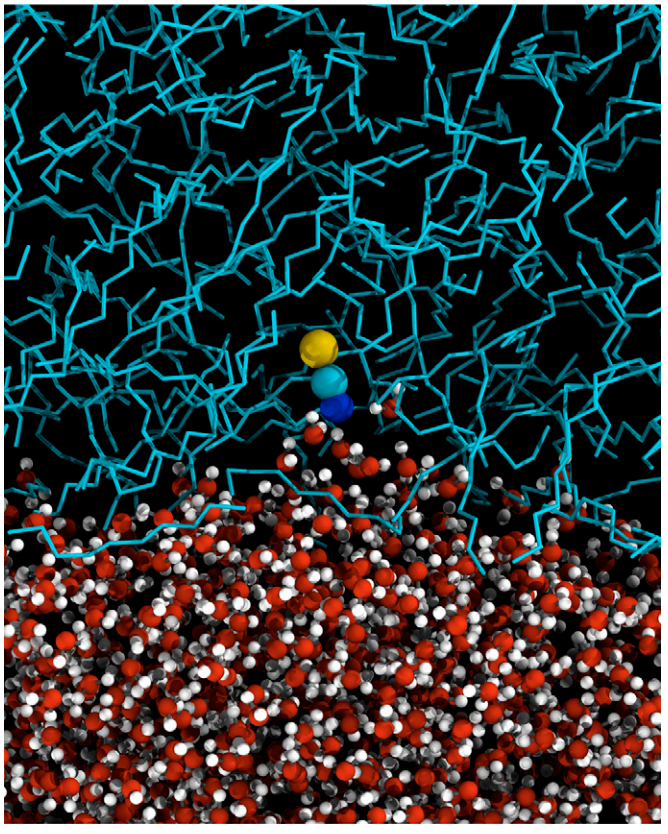

Fig. 6. A snapshot of the SCN^- ion (blue = N, green = C, yellow = S, image enlarged) adsorbed at the water-decane interface.

Materials and Methods

All glassware and sample dishes used were soaked overnight in AlNochromix (Alconox Inc.) cleaning solution and then rinsed thoroughly with 18.2 M Ω ultra-pure water. NaSCN salt (Alfa Aesar 98% minimum purity) was baked overnight in a 150 °C oven to remove organic impurities prior to making salt solutions. Toluene (Thermo Fisher Scientific, HPLC grade, 99.8% minimum purity) was purified with baked silica gel for SHG experiments and used unpurified for SFG experiments. Decane (Thermo Fisher Scientific, HPLC grade, 99.8% minimum purity) was used without purification for both SHG and SFG experiments. The NaSCN-hydrophobe interfaces were prepared by depositing NaSCN solution into a Petri dish and then depositing a thin layer of liquid hydrocarbon on top of the aqueous solution.

SHG Experimental Design. The output of a Ti-S amplified laser system (Spectra Physics Spitfire, 2 mJ, 1 kHz, 100 fs) centered at 800 nm is directed through an optical parametric amplifier (TOPAS) to generate light at 386 nm for water-toluene measurements and passed through a barium borate (BBO) crystal to generate light at 400 nm for water-decane measurements. The light is then focused onto the surface of a Petri dish containing the NaSCN solution and hydrocarbon surface layer, with input energies of 1–3 μJ per pulse, depending on solution concentration. The reflected SH photons are collected and spectrally filtered from the fundamental light by a Pellin-Broca prism and detected using a gated integration system (Stanford Research Systems), a monochromator (Acton SpectraPro 2150i), and a photomultiplier (Hamamatsu, R7154PHA) for photon counting. The polarization scheme used was *pp* (*p*-polarized SH, *p*-polarized fundamental). For each SHG measurement of NaSCN at the water-toluene or water-decane interface, a measurement was made for NaSCN at the air-water interface from the same aqueous solution. All measurements of NaSCN at a water-hydrophobe surface were normalized relative to the response of the respective pure water-hydrophobe interface.

SFG Experimental Design. The experimental setup has been described in detail previously (61). Briefly, a Ti-S amplified laser system (Spectra Physics Spitfire, 4 mJ, 1 kHz, 100 fs) centered at 800 nm is used to generate a broadband white light continuum pulse (WLC) (600-1,400 nm) and a narrowband UV pulse at 266 nm (FWHM = 2 nm).

The narrowband UV and broadband WLC pulses are overlapped temporally and spatially at the water-hydrocarbon surface to generate a sum-frequency (SF) photon in the phase-matched direction, enabling ~30 nm of spectral width (~190–220 nm) to be observed in a single laser shot. SF photons are collected and sent into a spectrograph (Acton SpectraPro 300i) and CCD (Princeton Instruments PIXIS 2K) for detection. Each raw NaSCN spectrum has a corresponding background spectrum that is generated by separating the two input pulses in time. Spectra of the neat water-hydrocarbon interface (no added SCN^-) were also collected with spatial and temporal overlap, for background subtraction. The polarization scheme used was *ppp* (*p*-polarized SFG, *p*-polarized 266 nm, *p*-polarized WLC). All interfacial spectra of NaSCN are normalized to

the nonresonant response from gallium arsenide (GaAs), which corrects for the low efficiency of optics in the short-wavelength region as well as lower intensities of the WLC on the edges of its spectrum.

MD Simulations. The liquid-liquid interface is formed by placing a slab of water molecules next to a slab of toluene or decane molecules in a rectangular box and is located in the *X-Y* plane at $Z \sim 0$. The water phase occupies the region $Z < 0$ and the oil phase is in the $Z > 0$ region. Each liquid phase is at equilibrium with its own vapor phase, so there is only one liquid-liquid interface. Periodic boundary conditions are applied in all directions. A reflecting wall is located 5 Å from the simulation box boundaries in the *Z*-direction to prevent mixing of the two vapor phases. The systems studied include a single SCN^- ion placed in different locations of the water-oil interface.

The potential energy functions used for water are a flexible version of the SPC model. For toluene, a fully atomistic flexible model based on the optimized potentials for liquid simulations (OPLS) all-atom description, and for decane, a united-atom OPLS model are used (62). The intermolecular interaction potentials are described as the pairwise sum of Lennard-Jones (LJ) and Coulomb terms. Standard Lorentz-Berthelot combining rules (63) are used to generate LJ parameters for the interactions between atoms located in different molecules. These parameters are given in the *SI Appendix*. The intermolecular SCN^- ion potential is taken from the work of Tesei at al. (64). This model was shown to reproduce several experimental data, including the air-water surface tension for a wide range of salt concentrations. In addition, we used a harmonic potential with parameters selected to reproduce the infrared (IR) fundamental frequencies of this ion in solution (65).

The simulation methodology used to examine the adsorption of ions at the liquid-liquid interface has been described in detail elsewhere (51). Briefly, the SCN^- ion is restricted by an external potential to be in *N* overlapping lamellas, each 2 Å wide, spanning the region from bulk water to bulk oil. In each lamella, a 5 ns constant temperature (T = 298 K) MD trajectory is carried out and used to compute the ion's position probability distribution and several structural and energetic properties of the ion as a function of the distance from the interface. The free energy profile for the adsorption of the ion is determined using the umbrella sampling method (51, 63) by combining the local free energy segments calculated from the ion's position probability distribution functions. All the MD simulations are performed with in-house software that uses the velocity Verlet algorithm (63) with an integration time-step of 1 fs.

Data, Materials, and Software Availability. Experimental second-harmonic generation and sum-frequency generation data, as well as molecular dynamics simulation data are available on the Figshare data repository (67).

ACKNOWLEDGMENTS. S.W.D. and R.J.S. are supported by the Department of Energy, Office of Basic Energy Sciences, through the Chemical Sciences Division at the Lawrence Berkeley National Laboratory under contract No. CH403503 and through the ACS Petroleum Research Fund under grant No. 59408-ND6. I.B. acknowledge the support of the NSF through grant CHE-1800158.

1. P. Jungwirth, D. J. Tobias, Ions at the air/water interface. *J. Phys. Chem. B* **106**, 6361–6373 (2002).
2. P. B. Petersen, R. J. Saykally, Confirmation of enhanced anion concentration at the liquid water surface. *Chem. Phys. Lett.* **397**, 51–55 (2004).
3. E. M. Knipping *et al.*, Experiments and simulations of ion-enhanced interfacial chemistry on aqueous NaCl aerosols. *Science* **288**, 301–306 (2000).
4. J. H. Hu *et al.*, Reactive uptake of Cl2 (g) and Br2 (g) by aqueous surfaces as a function of Br-and I-ion concentration: The effect of chemical reaction at the interface. *J. Phys. Chem.* **99**, 8768–8776 (1995).
5. B. A. Wellen, E. A. Lach, H. C. Allen, Surface pK_a of octanoic, nonanoic, and decanoic fatty acids at the air-water interface: Applications to atmospheric aerosol chemistry. *Phys. Chem. Chem. Phys.* **19**, 26551–26558 (2017).
6. A. M. Jubb, W. Hua, H. C. Allen, Organization of water and atmospherically relevant ions and solutes: Vibrational sum frequency spectroscopy at the vapor/liquid and liquid/solid interfaces. *Acc. Chem. Res.* **45**, 110–119 (2012).
7. T. L. Tarbuck, G. L. Richmond, Adsorption and reaction of CO_2 and SO_2 at a water surface. *J. Am. Chem. Soc.* **128**, 3256–3267 (2006).
8. Q. Du, E. Freysz, Y. R. Shen, Surface vibrational spectroscopic studies of hydrogen bonding and hydrophobicity. *Science* **264**, 826–828 (1994).
9. P. B. Miranda, Y. R. Shen, Liquid interfaces: A study by sum-frequency vibrational spectroscopy. *J. Phys. Chem. B* **103**, 3292–3307 (1999).
10. G. Ma, X. Chen, H. C. Allen, Dangling OD confined in a Langmuir monolayer. *J. Am. Chem. Soc.* **129**, 14053–14057 (2007).
11. L. F. Scatena, M. G. Brown, G. L. Richmond, Water at hydrophobic surfaces: Weak hydrogen bonding and strong orientation effects. *Science* **292**, 908–912 (2001).
12. S. Pullanchery, S. Kulik, S. Roke, Water structure at the hydrophobic nanodroplet surface revealed by vibrational sum frequency scattering using isotopic dilution. *J. Phys. Chem. B* **126**, 3186–3192 (2022).
13. R. Vácha *et al.*, The orientation and charge of water at the hydrophobic oil droplet-water interface. *J. Am. Chem. Soc.* **133**, 10204–10210 (2011).
14. D. L. McCaffrey *et al.*, Mechanism of ion adsorption to aqueous interfaces: Graphene/water vs. air/water. *Proc. Natl. Acad. Sci. U.S.A.* **114**, 13369–13373 (2017).
15. S. W. Devlin, D. L. McCaffrey, R. J. Saykally, Characterizing anion adsorption to aqueous interfaces: Toluene-water versus air-water. *J. Phys. Chem. Lett.* **13**, 222–228 (2022).
16. H. Wang, E. Borguet, K. B. Eisenthal, Generalized interface polarity scale based on second harmonic spectroscopy. *J. Phys. Chem. B* **102**, 4927–4932 (1998).
17. H. Wang, E. Borguet, K. B. Eisenthal, Polarity of liquid interfaces by second harmonic generation spectroscopy. *J. Phys. Chem. A* **101**, 713–718 (1997).
18. K. B. Eisenthal, Liquid interfaces probed by second-harmonic and sum-frequency spectroscopy. *Chem. Rev.* **96**, 1343–1360 (1996).
19. R. M. Onorato, D. E. Otten, R. J. Saykally, Measurement of bromide ion affinities for the air/water and dodecanol/water interfaces at molar concentrations by UV second harmonic generation spectroscopy. *J. Phys. Chem. C* **114**, 13746–13751 (2010).
20. R. M. Onorato, D. E. Otten, R. J. Saykally, Adsorption of thiocyanate ions to the dodecanol/water interface characterized by UV second harmonic generation. *Proc. Natl. Acad. Sci. U.S.A.* **106**, 15176–15180 (2009).
21. P. Jungwirth, D. J. Tobias, Specific ion effects at the air/water interface. *Chem. Rev.* **106**, 1259–1281 (2006).
22. S. J. Stuart, B. J. Berne, Effects of polarizability on the hydration of the chloride ion. *J. Phys. Chem.* **100**, 11934–11943 (1996).
23. D. E. Otten, P. R. Shaffer, P. L. Geissler, R. J. Saykally, Elucidating the mechanism of selective ion adsorption to the liquid water surface. *Proc. Natl. Acad. Sci. U.S.A.* **109**, 701–705 (2012).
24. J. Noah-Vanhoucke, P. L. Geissler, On the fluctuations that drive small ions toward, and away from, interfaces between polar liquids and their vapors. *Proc. Natl. Acad. Sci. U.S.A.* **106**, 15125–15130 (2009).
25. T.-M. Chang, L. X. Dang, Recent advances in molecular simulations of ion solvation at liquid interfaces. *Chem. Rev.* **106**, 1305–1322 (2006).
26. Y. Levin, A. P. dos Santos, Ions at hydrophobic interfaces. *J. Phys. Condens. Matter* **26**, 203101 (2014).
27. Y. Wang, S. Sinha, P. R. Desai, H. Jing, S. Das, Ion at air-water interface enhances capillary wave fluctuations: Energetics of ion adsorption. *J. Am. Chem. Soc.* **140**, 12853–12861 (2018).
28. L. Sun, X. Li, Y. Tu, H. Ågren, Origin of ion selectivity at the air/water interface. *Phys. Chem. Chem. Phys.* **17**, 4311–4318 (2015).
29. S. J. Cox, D. G. Thorpe, P. R. Shaffer, P. L. Geissler, Assessing long-range contributions to the charge asymmetry of ion adsorption at the air-water interface. *Chem. Sci. (Camb.)* **11**, 11791–11800 (2020).
30. C. L. McFearin, D. K. Beaman, F. G. Moore, G. L. Richmond, From Franklin to today: Toward a molecular level understanding of bonding and adsorption at the oil- water interface. *J. Phys. Chem. C* **113**, 1171–1188 (2009).
31. L. Lin *et al.*, Ion pairing mediates molecular organization across liquid/liquid interfaces. *ACS Appl. Mater. Interfaces* **13**, 33734–33743 (2021).
32. L. Lin *et al.*, Ion pairing and molecular orientation at liquid/liquid interfaces: Self-assembly and function. *J. Phys. Chem. B* **126**, 2316–2323 (2022).
33. D. M. Mitrinović, A. M. Tikhonov, M. Li, Z. Huang, M. L. Schlossman, Noncapillary-wave structure at the water-alkane interface. *Phys. Rev. Lett.* **85**, 582–585 (2000).
34. D. M. Mitrinovic, Z. Zhang, S. M. Williams, Z. Huang, M. L. Schlossman, X-ray reflectivity study of the water-hexane interface. *J. Phys. Chem. B* **103**, 1779–1782 (1999).
35. G. Luo *et al.*, Ion distributions near a liquid-liquid interface. *Science* **311**, 216–218 (2006).
36. A. P. Willard, D. Chandler, The molecular structure of the interface between water and a hydrophobic substrate is liquid-vapor like. *J. Chem. Phys.* **141**, 18C519 (2014).
37. J. J. Karnes, N. Villavicencio, I. Benjamin, Transfer of an erbium ion across the water/dodecane interface: Structure and thermodynamics via molecular dynamics simulations. *Chem. Phys. Lett.* **737**, 136825 (2019).
38. M. J. Servis, A. E. Clark, Surfactant-enhanced heterogeneity of the aqueous interface drives water extraction into organic solvents. *Phys. Chem. Chem. Phys.* **21**, 2866–2874 (2019).
39. N. Kumar, M. J. Servis, Z. Liu, A. E. Clark, Competitive interactions at electrolyte/octanol interfaces: A molecular perspective. *J. Phys. Chem. C* **124**, 10924–10934 (2020).
40. Y. Ghadar, S. L. Christensen, A. E. Clark, Influence of aqueous ionic strength upon liquid: Liquid interfacial structure and microsolvation. *Fluid Phase Equilib.* **407**, 126–134 (2016).
41. M. F. Fox, C. B. Smith, E. Hayon, Far-ultraviolet solution spectroscopy of thiocyanate. *J. Chem. Soc. Faraday Trans. 1 Phys. Chem. Condens. Phases* **77**, 1497–1502 (1981).
42. D. Bhattacharyya *et al.*, New insights into the charge-transfer-to-solvent spectrum of aqueous iodide: Surface versus bulk. *J. Phys. Chem. Lett.* **11**, 1656–1661 (2020).
43. H. Mizuno, A. M. Rizzuto, R. J. Saykally, Charge-transfer-to-solvent spectrum of thiocyanate at the air/water interface measured by broadband deep ultraviolet electronic sum frequency generation spectroscopy. *J. Phys. Chem. Lett.* **9**, 4753–4757 (2018).
44. S. K. Paul, J. M. Herbert, Probing interfacial effects on ionization energies: The surprising banality of anion-water hydrogen bonding at the air/water interface. *J. Am. Chem. Soc.* **143**, 10189–10202 (2021).
45. H. I. Okur, Y. Chen, D. M. Wilkins, S. Roke, The Jones-Ray effect reinterpreted: Surface tension minima of low ionic strength electrolyte solutions are caused by electric field induced water-water correlations. *Chem. Phys. Lett.* **684**, 433–442 (2017).
46. S. N. Wren, D. J. Donaldson, Glancing-angle Raman spectroscopic probe for reaction kinetics at water surfaces. *Phys. Chem. Chem. Phys.* **12**, 2648–2654 (2010).
47. V. Venkateshwaran, S. Vembanur, S. Garde, Water-mediated ion-ion interactions are enhanced at the water vapor-liquid interface. *Proc. Natl. Acad. Sci. U.S.A.* **111**, 8729–8734 (2014).
48. P. B. Petersen, R. J. Saykally, Evidence for an enhanced hydronium concentration at the liquid water surface. *J. Phys. Chem. B* **109**, 7976–7980 (2005).
49. B. V. P. Sokhan, D. J. Tildesley, The free surface of water: Molecular orientation, surface potential and nonlinear susceptibility. *Mol. Phys.* **92**, 625–640 (1997).

50. J. S. Rowlinson, B. Widom, *Molecular Theory of Capillarity* (Courier Corporation, 2013).
51. I. Benjamin, Reaction dynamics at liquid interfaces. *Annu. Rev. Phys. Chem.* **66**, 165–188 (2015).
52. L. Benjamin, Mechanism and dynamics of ion transfer across a liquid-liquid interface. *Science* **261**, 1558–1560 (1993).
53. A. A. Kornyshev, A. M. Kuznetsov, M. Urbakh, Coupled ion–interface dynamics and ion transfer across the interface of two immiscible liquids. *J. Chem. Phys.* **117**, 6766–6779 (2002).
54. N. Kikkawa, L. Wang, A. Morita, Microscopic barrier mechanism of ion transport through liquid-liquid interface. *J. Am. Chem. Soc.* **137**, 8022–8025 (2015).
55. J. J. Karnes, I. Benjamin, Geometric and energetic considerations of surface fluctuations during ion transfer across the water-immiscible organic liquid interface. *J. Chem. Phys.* **145**, 014701 (2016).
56. A. Morita, A. Koizumi, T. Hirano, Recent progress in simulating microscopic ion transport mechanisms at liquid-liquid interfaces. *J. Chem. Phys.* **154**, 080901 (2021).
57. I. Benjamin, Molecular dynamics studies on the effect of surface roughness and surface tension on the thermodynamics and dynamics of hydronium ion transfer across the liquid/liquid interface. *J. Phys. Chem. B* **124**, 8711–8718 (2020).
58. F. Bresme, E. Chacón, P. Tarazona, K. Tay, Intrinsic structure of hydrophobic surfaces: The oil-water interface. *Phys. Rev. Lett.* **101**, 056102 (2008).
59. I. Schlesinger, U. Sivan, Three-dimensional characterization of layers of condensed gas molecules forming universally on hydrophobic surfaces. *J. Am. Chem. Soc.* **140**, 10473–10481 (2018).
60. N. N. Nguyen, A. V. Nguyen, K. M. Steel, L. X. Dang, M. Galib, Interfacial gas enrichment at hydrophobic surfaces and the origin of promotion of gas hydrate formation by hydrophobic solid particles. *J. Phys. Chem. C* **121**, 3830–3840 (2017).
61. A. M. Rizzuto, S. Irgen-Gioro, A. Eftekhari-Bafrooei, R. J. Saykally, Broadband deep UV spectra of interfacial aqueous iodide. *J. Phys. Chem. Lett.* **7**, 3882–3885 (2016).
62. W. Damm, A. Frontera, J. Tirado–Rives, W. L. Jorgensen, OPLS all-atom force field for carbohydrates. *J. Comput. Chem.* **18**, 1955–1970 (1997).
63. D. J. Tildesley, M. P. Allen, *Computer Simulation of Liquids* (Clarendon, Oxford, 1987).
64. G. Tesei, V. Aspelin, M. Lund, Specific cation effects on SCN^- in bulk solution and at the air-water interface. *J. Phys. Chem. B* **122**, 5094–5105 (2018).
65. L. H. Jones, Infrared spectrum and structure of the thiocyanate ion. *J. Chem. Phys.* **25**, 1069–1072 (1956).
66. I. Benjamin, Structure, thermodynamics, and dynamics of thiocyanate ion adsorption and transfer across the water/toluene interface. *J. Phys. Chem. B* **126**, 5706–5714 (2022).
67. S.W. Devlin, R. J. Saykally, I. Benjamin, On The Mechanism of Ion Adsorption to Aqueous Interfaces (2022) https://doi.org/10.6084/m9.figshare.20452242.v2 (September 30, 2022).